

Energy Storage

Facile Green Synthesis of BCN Nanosheets as High-Performance Electrode Material for Electrochemical Energy Storage

Indrapal Karbhal,^[a, b] Rami Reddy Devarapalli,^[a, b] Joyashish Debgupta,^[a] Vijayamohan K. Pillai,^[b, c, d] Pulickel M. Ajayan,^[e] and Manjusha V. Shelke^{*[a, b, c, e]}

Abstract: Two-dimensional hexagonal boron carbon nitride (BCN) nanosheets (NSs) were synthesized by new approach in which a mixture of glucose and an adduct of boric acid (H_3BO_3) and urea (NH_2CONH_2) is heated at 900 °C. The method is green, scalable and gives a high yield of BCN NSs with average size of about 1 μm and thickness of about 13 nm. Structural characterization of the as-synthesized ma-

terial was carried out by several techniques, and its energy-storage properties were evaluated electrochemically. The material showed excellent capacitive behaviour with a specific capacitance as high as 244 Fg^{-1} at a current density of 1 Ag^{-1} . The material retains up to 96% of its initial capacity after 3000 cycles at a current density of 5 Ag^{-1} .

Introduction

Two-dimensional (2D) nanomaterials have attracted much attention in recent years due to their unique planar structure with remarkable physical, chemical and electronic properties as a function of layer thickness. Among 2D materials, especially graphene and its inorganic analogues, such as h-BN, BCN, titanium carbide, MoS_2 and WS_2 , have been the focus of materials research.^[1–3] Of these materials, graphene is the most studied. It has a layered structure consisting of sp^2 -hybridized carbon atoms arranged in a hexagonal crystal lattice and has unique optical and electronic properties.^[4–6] Layered 2D BCN sheets have similar structure and mechanical, electronic and thermal properties to graphene doped with B and N. B and N are neighbours of C, and their atomic radii (B: 87 pm, C: 67 pm and N: 56 pm) and electronegativities (B: 2.04, C: 2.55 and N: 3.04) are similar to those of C. Thus, they can undergo strong covalent bonding with C and can form highly thermodynamically

stable, lighter-weight BCN compounds, which are more favourable and promising for various applications.^[7–10]

BCN, which is often conceptually thought of as a hybrid of graphene and hexagonal BN, has the properties anticipated for an adduct of these two materials. However, it has various structural forms with compositions such as BCN, BC_2N , BC_3N , BC_4N and BC_6N , depending on the relative percentages of B and N.^[11–15] Generally, B introduces holes and N introduces electrons into the carbon lattice, rendering the BCN to a p-type or n-type narrow-gap semiconductor, respectively.

BCN has very attractive properties, such as suitable bandgap, luminescence, cathodoluminescence, electroluminescence, thermoelectricity, low frictional coefficient and high neutron-absorbing capability. Therefore, it has been widely considered for catalysis, sensors, neutron absorbers, protective coatings, gas absorption, electrocatalysts for the oxygen reduction reaction (ORR) and as energy-storage material for batteries and supercapacitors. The presence of heteroatoms (B and N) plays a key role in enhancing the performance in many of these applications and improving the stability, similar to the cases of graphene and other 2D materials.^[16–18]

However, synthetic methods for the production of BCN are not well developed. Chemical vapour deposition, pyrolysis, dc arc discharge and laser ablation are some of the methods reported so far for the preparation of BCN. Almost, all techniques require high temperature, sophisticated instrumentation or costly chemicals. Moreover, the very low yields of BCN make these techniques quite impractical in real-life applications.^[13, 19–25] Polymer-precursor-based synthesis of BCN has been reported by Zhang et al., although there are a few concerns such as inadequate purity and dimensional homogeneity.^[26] In contrast to these methods, the present work reports a facile synthesis of BCN NSs by employing boric acid, urea and glucose as B, N and C sources, respectively, as high-performance supercapacitor electrode materials.

[a] I. Karbhal, R. R. Devarapalli, J. Debgupta, M. V. Shelke
Physical & Materials Chemistry Division
CSIR-National Chemical Laboratory (CSIR-NCL)
Pune 411008, MH (India)
E-mail: mv.shelke@ncl.res.in

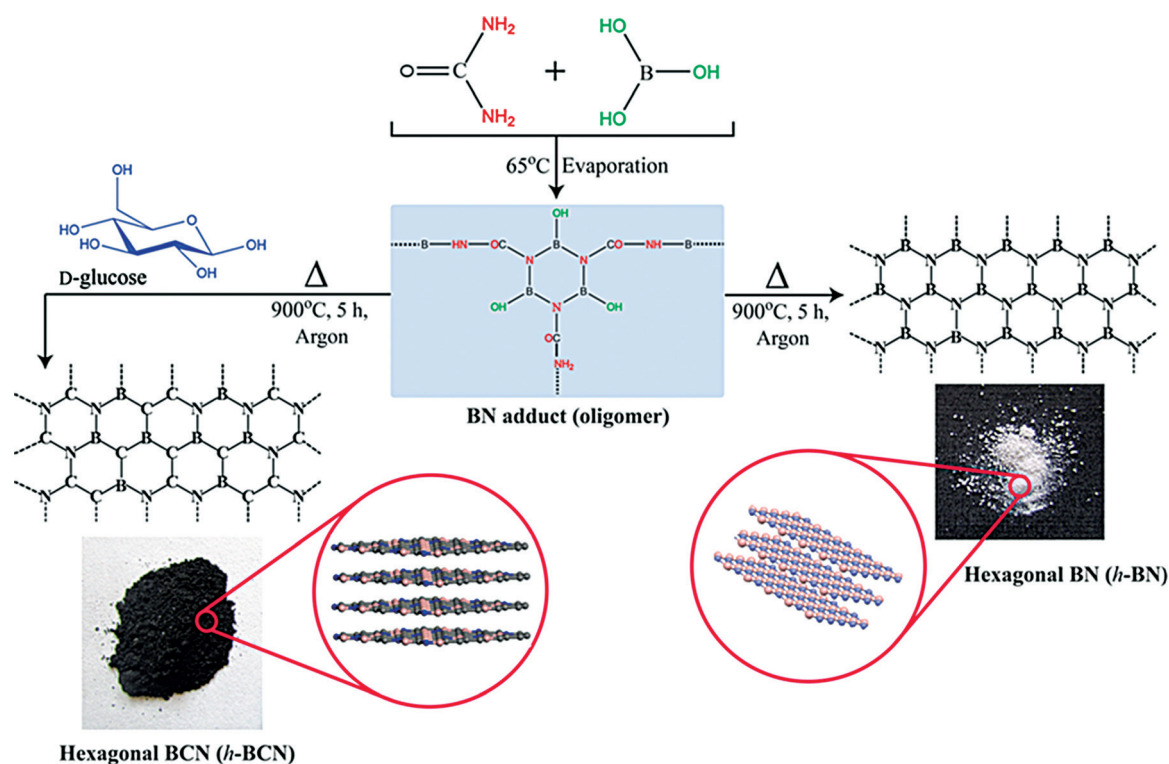
[b] I. Karbhal, R. R. Devarapalli, V. K. Pillai, M. V. Shelke
Academy of Scientific and Innovative Research (AcSIR)
Chennai 600113, TN (India)

[c] V. K. Pillai, M. V. Shelke
CSIR-Network Centre for Solar Energy, CSIR-NCL, Pune (India)

[d] V. K. Pillai
CSIR-Central Electrochemical Research Institute (CSIR-CECRI)
Karaikudi 630006 (India)

[e] P. M. Ajayan, M. V. Shelke
Department of Mechanical Engineering & Material Science
Rice University, Houston 77005 TX (USA)

Supporting information for this article is available on the WWW under <http://dx.doi.org/10.1002/chem.201505225>.



Scheme 1. Schematic representation of the overall synthetic route for the preparation of h-BCN and h-BN.

The advantages of this method is that, it is green, scalable, occurs at relatively low temperature (900 °C) compared to previously reported methods,^[12,14,27] requires no catalyst and, above all, uses cheap and readily available precursors. First, an adduct of boric acid and urea was prepared by heating at 65 °C. Subsequent heating of this adduct with glucose at 900 °C produces BCN sheets. Three different types of BCN composites were synthesized by varying the initial ratio of BN adduct to glucose and named BCN (3:1), BCN (1:1) and BCN (1:3). Scheme 1 describes the overall process for the synthesis of hexagonal BCN (h-BCN). The products were characterized by Fourier transform infra red (FTIR) spectroscopy, Raman spectroscopy, Scanning Electron Microscope (SEM), Transmission Electron Microscope (TEM), powder X-ray diffraction (PXRD), X-ray photoelectron spectroscopy (XPS) and Brunauer, Emmett and Teller (BET) surface area analysis.

Despite its being a highly important material, BCN has not been widely explored in the field of energy. Recently, Wang et al. have shown BCN/graphene to be a good electrocatalyst for the ORR.^[17] Lei et al. have synthesized BCN NSs in a molten mixture of LiCl and KCl using NaBH₄ and urea as B and C, N sources, respectively, for application in Li-ion batteries.^[28] Very few reports are available on energy-storage applications of BCN. Vertically aligned BCN nanotubes are reported to show a specific capacitance of 321 Fg⁻¹ at a current density of 0.2 Ag⁻¹.^[29] However, the current density applied to achieve this capacitance is very low in terms of practical applications, in which supercapacitors are required to charge and discharge at very high rates. More significantly, the possible destruction of the alignment by sustained electric field during the charge/

discharge operation of the supercapacitor and the consequent performance deterioration have not been discussed. On the other hand, the BCN synthesized by the present method shows a specific capacitance as high as 244 Fg⁻¹ at a high current density of 1 Ag⁻¹ with much more robust performance and higher rate capability. For example, it shows excellent stability and capacitance retention ($\approx 96\%$) even at a higher current density (5 Ag⁻¹).

Results and Discussion

Figure 1 A shows representative PXRD patterns of BCN with different B and N contents. The PXRD pattern of glucose-derived carbon (obtained by heating glucose in Ar at 900 °C) is also shown for comparison. Interestingly, the (002) and (100) planes are mostly exposed in all three different types of h-BCN, and the highest intensity is seen for the peak corresponding to the (002) plane (JCPDS Card No. 35-1292). More significantly, the position of this peak shifts slowly towards lower 2θ values with increasing B and N content compared to that of glucose-derived carbon. This peak appears at 25.8° for glucose-derived carbon, whereas all the BCN samples show 2θ between 24.8 and 25.3° for the (002) plane. The peak positions for BCN match well with the pattern reported previously.^[19] As shown in Figure 1A, the *d* spacing of the BCN increases with increasing ratio of BN adduct to glucose, probably because N is smaller in size than C, and B is more electrophilic in nature and tends to form stronger covalent bonds with C and N.

Raman spectroscopy was also used for structure analysis (Figure 1B). All the as-obtained BCN NSs samples show two

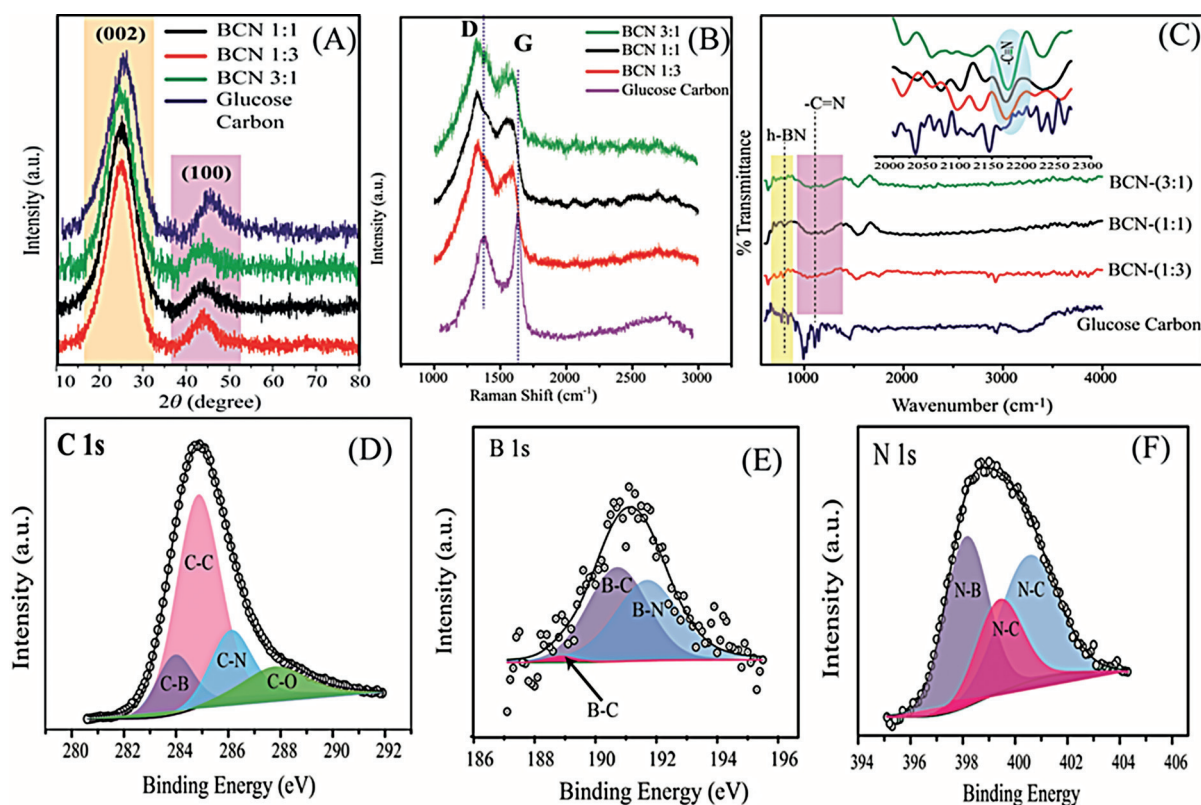


Figure 1. A) PXRD pattern of BCN NSs having BN:C ratios of 1:1, 1:3 and 3:1 as well as glucose-derived carbon. B) Raman spectra of BCN NSs and glucose-derived carbon. C) FTIR spectra of BCN and glucose-derived carbon (Glucose Carbon); inset: enlarged view of the IR spectra showing the $C\equiv N$ stretching band. D)–F) Representative core-level C 1s, N 1s and B 1s XPS spectra of BCN (3:1) showing the presence of C–C, C–B, C–N and B–N bonds (open circles: raw data, solid line: overall fit, coloured areas: deconvoluted peaks).

characteristic peaks, namely, the D or defect-induced band and G or graphitic band at 1325 and 1572 cm^{-1} , respectively. The D and G bands are redshifted by about 10 cm^{-1} compared to those of glucose-derived carbon. Redshifting of both D and G bands of BCN compared to that of glucose-derived carbon indicates heterogeneity in BCN because of the presence of B–C, C–N and B–N bonds. Since, N doping introduces electrons and B doping holes into the carbon matrix, both processes result in changes in the electronic structure of carbon matrix, which lead to changes in the polarization in the material and cause shifts in the Raman spectra. The D-band shift is attributed to the introduction of new types of disorders due to the new fine structures in the system, whereas shifts in the G band are due to weakening of C–C bonds by elongation or contraction, which results in changes in the electronic structure. Further, the codoping of B and N in the carbon matrix introduces excess electron carriers and thereby causes the redshift compared to glucose-derived carbon. This is also evident in the I_D/I_G ratio, which is higher in BCN than in glucose-derived carbon. For comparison, Raman spectra of the BN adduct and h-BN are shown in Figure S1 of the Supporting Information. In the case of the BN adduct no peak was detected, but in the case of h-BN one distinct peak appeared at 1371 cm^{-1} (Supporting Information, Figure S1).^[19,30,31]

Figure 1C shows superimposed FTIR spectra of BCN NSs and glucose-derived carbon to reveal the common features. For example, the peak at 785 cm^{-1} is due to the presence of B–N bonds in BCN, and the broad peak between 1100 and 1250 cm^{-1} is due to the C=N stretching vibration. In contrast, both of these peaks are absent in the spectrum of glucose-derived carbon. However, the inset of Figure 1C shows the $C\equiv N$ stretching band for BCN at 2170 cm^{-1} , which confirms the formation of a ternary BCN compound.^[25]

XPS is a valuable tool for confirming the presence of B–C, C–N, B–N and C–C bonds in BCN. The survey spectrum of BCN (3:1) is shown in Figure S2 of the Supporting Information. Since XPS is a surface analysis technique, we observed the presence of B, C, N and O in the survey scan. The presence of O in the survey scan could be due to moisture adsorbed on the surface owing to the strongly oxophilic nature of B in the material. From the deconvolution of the corresponding peak of C, information on the bonding of C was obtained. Accordingly, Figure 1D shows a C 1s signal that can be deconvoluted into four peaks at 283.9 , 284.8 , 286.1 and 287.8 eV , which are assigned to C–B, C–C, C–N and C–O bonds, respectively. Figure 1E shows the N 1s signal, which is the sum of three peaks at 398.1 , 399.4 and 400.5 eV . These peaks correspond to N–B, graphitic N–C, and pyridinic N–C bonds, respectively. Figure 1F

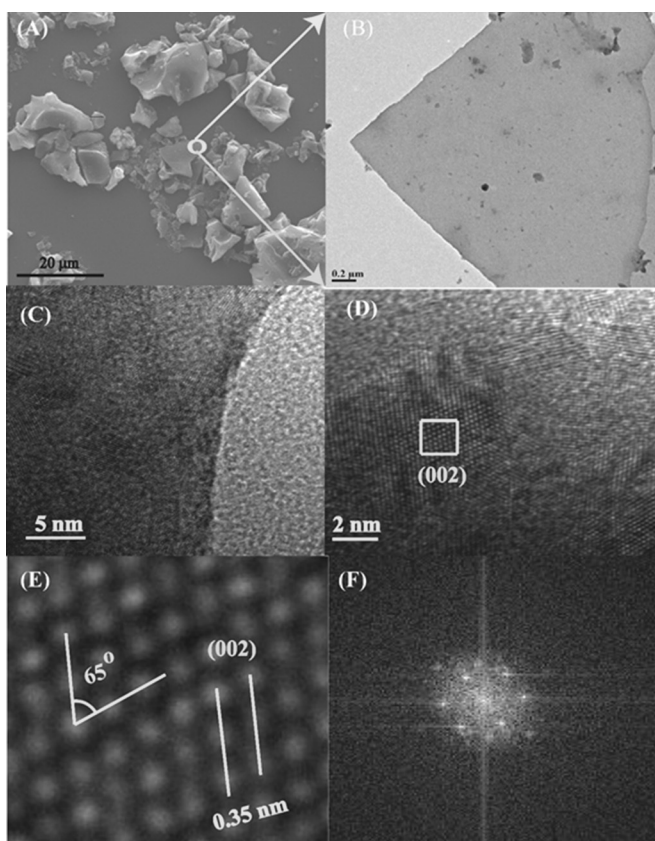


Figure 2. A) SEM and B) TEM images of BCN (3:1) showing sheet-like morphology. C) and D) High-resolution TEM images of a portion of the BCN sheet revealing lattice fringes (E) and corresponding fast Fourier transform pattern (F)

shows the B 1s signal, which can be deconvoluted into three peaks due to B–C, B=C and B–N bonds at 189, 190.7 and 191.7 eV, respectively. All the peaks thus suggest the formation of B–C, C–C, C–N and B–N bonds.^[29]

Figure 2A shows a representative SEM image of as-synthesized BCN (3:1). The high-resolution (HR) TEM image in Figure 2B reveals a sheet-like structure of the material. Lattice fringes are visible at higher magnification, and the *d* spacing calculated from the lattice fringes is 0.35 nm, which matches well with that of the (002) plane of hexagonal BCN in the XRD pattern (JCPDS No. 35-1292). On the other hand, the inset of Figure 2D clearly shows two interconnecting planes. The angle between these two planes is 65°. The fast Fourier transform image in Figure 2F indicates formation of a hexagonal structure.^[32] SEM and TEM images of BCN (3:1), BCN (1:1) and BCN (1:3) and glucose-derived carbon are shown in Figures S3 and S4 of the Supporting Information.

In addition, SEM imaging of as-prepared BCN NSs was performed, and elemental-mapping images for B, C and N are shown in Figure 3B–D, respectively. They indicate uniform distribution of B, C and N in the BCN NSs.

Atomic Force Microscope (AFM) imaging was performed to determine the thickness and size of the as-prepared BCN NSs (Figure 4). The size of the BCN NSs is about 1 μm and their thickness is about 13 nm.

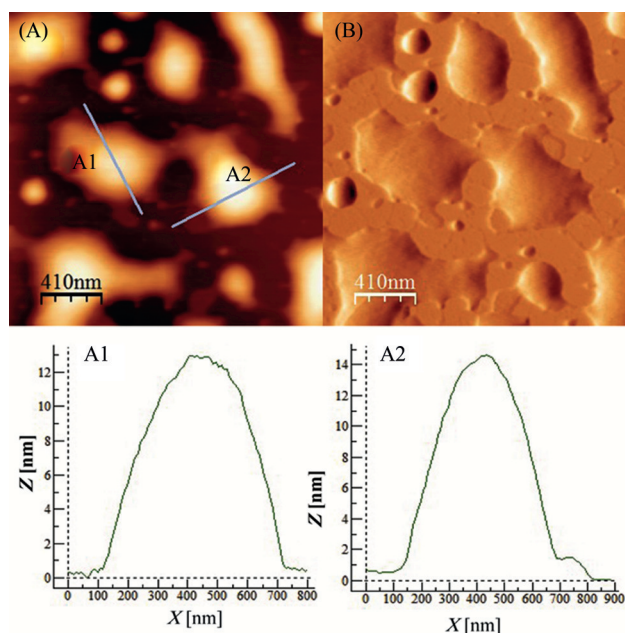


Figure 3. AFM images of BCN (3:1) and corresponding height profiles.

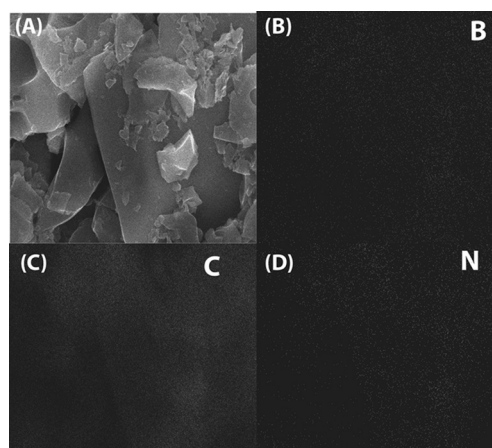


Figure 4. SEM image (A) and elemental mapping images for of B (B), C (C) and N (D).

Cyclic voltammetry (CV) and galvanostatic charge/discharge measurements were done by using 1 M H₂SO₄ as electrolyte in a two-electrode system. Figure 5A shows the CV curves of glucose-derived carbon and BCN (3:1), BCN (1:1) and BCN (1:3) at a typical scan rate of 100 mV s⁻¹ in 1 M H₂SO₄ solution. The CV measurements indicate a higher capacitance of BCN (3:1) compared to BCN (1:1), BCN (1:3) and glucose-derived carbon. Glucose-derived carbon shows a lower current and a smaller width of the CV curve implying low-capacitance behaviour. The capacitance increases systematically with increasing amount of BN adduct and, interestingly, the capacitance seems to be the highest for the case of BCN (3:1). This is also confirmed by Figure 5B, which shows typical galvanostatic charge/discharge curves at 1 A g⁻¹ for all BCN compositions and glucose-derived carbon and demonstrates that BCN (3:1) has

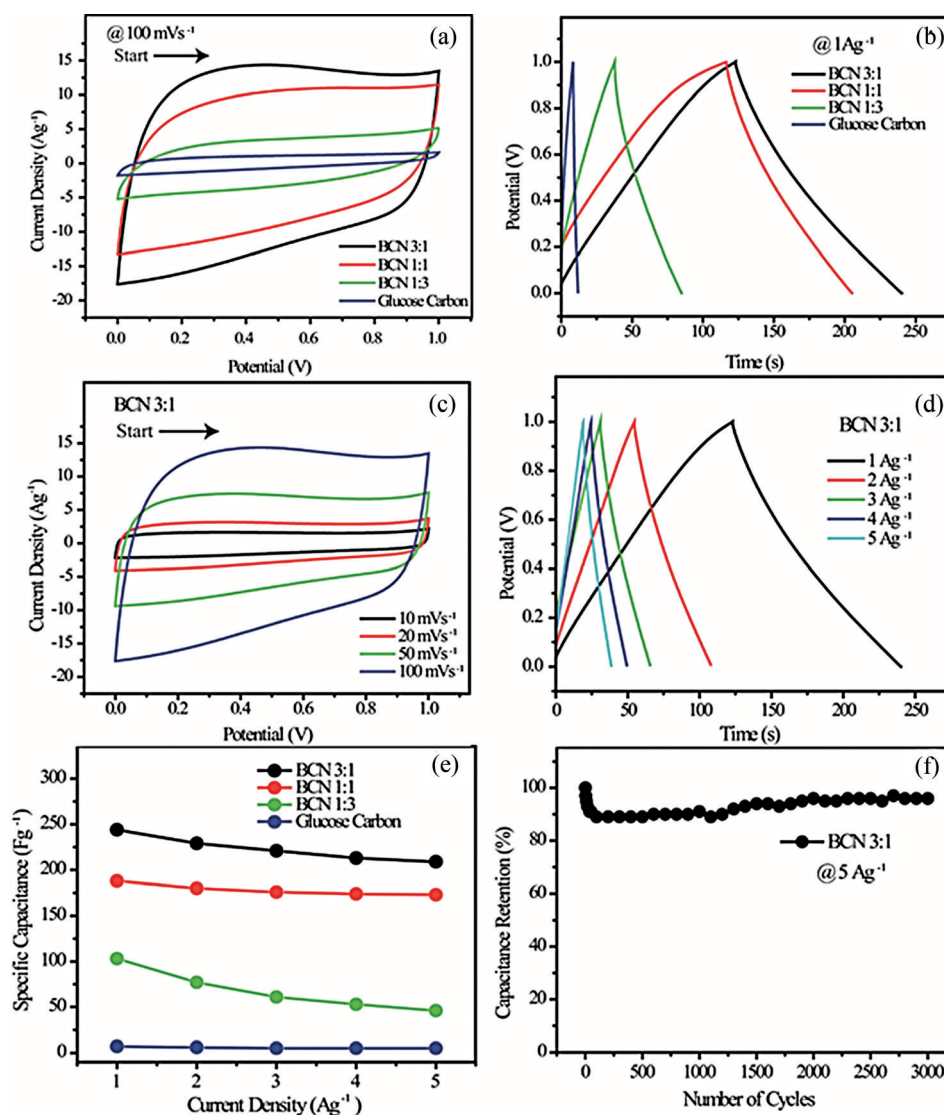


Figure 5. A) CV curves of glucose-derived carbon and BCN NSs with different compositions at 100 mVs^{-1} . B) Galvanostatic charge/discharge curves of glucose-derived carbon and BCN NSs. C) CV curves of BCN (3:1) at scan rates of 10, 20, 50 and 100 mVs^{-1} . D) Galvanostatic charge/discharge curves of BCN (3:1) at current densities of 1, 2, 3, 4 and 5 Ag^{-1} in $1 \text{ M H}_2\text{SO}_4$. E) Specific capacitance of glucose-derived carbon and BCN NSs with different compositions at current densities of 1, 2, 3, 4 and 5 Ag^{-1} . F) Stability evolution of BCN (3:1) at a current density of 5 Ag^{-1} in $1 \text{ M H}_2\text{SO}_4$.

a higher specific capacitance than the other BCN NSs and glucose-derived carbon.

The specific capacitances calculated from charge/discharge data for BCN (3:1), BCN (1:1), BCN (1:3) and glucose-derived carbon are 244 , 188 , 103 and 7 Fg^{-1} , respectively. The primary reason for the observed increase in capacitance with increasing fraction of BN adduct could be determined by measuring the chemical composition as well as surface area of as synthesized BCN.

The surface area of the BCN NSs was measured by BET analysis (Supporting Information, Table S1 and Figure S5). The BET surface area of BCN (3:1) of $314 \text{ m}^2\text{g}^{-1}$ is similar to that of BCN (1:1) ($343 \text{ m}^2\text{g}^{-1}$). BCN (1:3) and glucose-derived carbon have surface areas of 107 and $10 \text{ m}^2\text{g}^{-1}$, respectively. The pore volume of BCN (3:1) is $0.18 \text{ cm}^3\text{g}^{-1}$, whereas BCN (1:1), BCN (1:3) and glucose-derived carbon show pore volumes of 0.14 ,

0.042 and $0.018 \text{ cm}^3\text{g}^{-1}$ respectively. The higher capacitance of BCN (3:1) could be due to slightly higher pore volume and the chemical composition, because BCN (3:1) has a higher content of B, which plays a key role in incorporating ions on the surface of the electrode, which results in more diffusion and an increase in capacitance. B acts as an electrophilic centre; due to the presence of an empty p orbital it can store more charge by attracting ions electrostatically. Simultaneous N doping would lead to a combination of holes and electrons to enhance capacitance with increasing content of B and N in the carbon lattice to a certain extent. This combination of heteroatoms improves the performance of the material significantly, as illustrated by the data presented in Figure 5a and b.^[33–34] Figure 5c shows the CV curves of BCN (3:1) at scan rates of 10, 20, 50 and 100 mVs^{-1} in $1 \text{ M H}_2\text{SO}_4$ solution, and Figure 5d the galvanostatic charge/discharge curves of BCN (3:1) at 1, 2, 3, 4

and 5 Ag^{-1} . The capacitance of BCN (3:1) is 244 Fg^{-1} at a current density of 1 Ag^{-1} in $1 \text{ M H}_2\text{SO}_4$. To demonstrate the rate capability, Figure 5e shows the capacitance behaviour of glucose-derived carbon and BCN (3:1), (1:1) and (1:3) at current densities of 1, 2, 3, 4 and 5 Ag^{-1} . The usefulness of these electrode materials is further confirmed by the data in Figure 5f, which reveals durability of BCN (3:1) at a high current density of 5 Ag^{-1} with 96% retention of capacitance and excellent cycling stability, which confirm that BCN is a superior material for supercapacitor applications.

Electrochemical impedance spectroscopy (EIS) was carried out for all the BCN NSs, and the corresponding Nyquist plots are shown in Figure S6 of the Supporting Information. The straight line in the low-frequency region corresponding to the diffusion process is due to the capacitive behaviour of the BCN NSs. However, BCN (3:1) has a straight line in the lower-frequency region and also shows more pronounced capacitive behavior than the other BCN NSs in this study. The Nyquist plots also showed that the series resistance of the BCN NSs decreases with increasing amount of BN. This might be due to the more electrophilic nature of the material. Semicircles observed for BCN (3:1) and BCN (1:1) in the higher-frequency region are due to the electrochemical charge-transfer resistance at the electrode/electrolyte interface. The charge-transfer resistance of BCN (3:1) is lower than those of BCN (1:1) and BCN (1:3). From the EIS studies, it can be concluded that BCN (3:1) shows pronounced capacitive behaviour and lower electrochemical charge-transfer resistance. TEM imaging and XPS analysis were performed on the BCN nanosheets after electrochemical analysis to reveal any possible structural changes in the BCN NSs. The TEM image and selected-area electron diffraction pattern are shown in Figure S7 of the Supporting Information. The TEM image shows that after electrochemical studies the sheet-like morphology of BCN is not damaged much. SAED clearly showed a hexagonal pattern, the same as obtained for BCN sheets before the electrochemical studies. XP spectra of BCN nanosheets taken after electrochemical studies are shown in Figure S8 of the Supporting Information. The XPS data indicate that the B–C, B–N and C–C bonds remain stable after electrochemical tests, but an additional peak corresponding to C–OH is observed.

Thus, all the above data suggest the successful preparation of BCN NSs by employing easily available sources (boric acid, urea and glucose). As-synthesized BCN NSs were found to be potentially useful for supercapacitor applications with a very high specific capacitance of 244 Fg^{-1} , especially suitable for hybrid applications at higher power density. However, it is very difficult to precisely control the exact layer thickness of BCN NSs prepared by the current method, and it is difficult to obtain large integrated sheets. A controlled layer-by-layer bottom-up approach may alleviate these limitations in the future.

Conclusion

BCN NSs were synthesized with various ratios of BN adduct to glucose. The structure and supercapacitor performance of the

BCN NSs were studied systematically. SEM and HRTEM images showed a thin, sheet-like morphology with a hexagonal crystal lattice, and AFM showed that the sheet size is about $1 \mu\text{m}$ and the thickness of the nanosheets is around 13 nm. XPS confirmed the presence of C–C, B–C, B–N and C–N bonds. The capacitance increased with increasing fraction of the BN adduct to a certain extent, perhaps due to synergetic effects of codoped B and N. The excellent retention of capacitance (96%) at a current density of 5 Ag^{-1} after 3000 cycles indicates that BCN NSs have good stability and also high rate capability. BCN NSs show a consistent specific capacitance of 244 Fg^{-1} at a current density of 1 Ag^{-1} , which is superior to those of other promising materials for supercapacitors.

Experimental Section

Materials

α -D-Glucose was procured from Sigma-Aldrich. Boric acid and urea were obtained from Lobachem. All chemicals were used as received.

Synthesis of BCN nanosheets

Boric acid and urea were used as boron and nitrogen precursors, respectively, and glucose was used as a primary carbon source. Typically, for the synthesis of BCN nanosheets, BN adduct was first prepared by mixing boric acid and urea in a molar ratio of 1:48. The mixture of urea and boric acid was then slowly heated at 65°C until white needle-shaped crystals of the BN adduct formed.^[35,36] The BN adduct was mixed with glucose in three different weight ratios (BN:C=1:1, 1:3, 3:1) by grinding in a mortar and pestle. The mixture was then heated at 900°C for 5 h under argon atmosphere. For the comparisons of structure and electrochemical performance, glucose and BNs adduct were heated separately at 900°C to obtain carbon and h-BN respectively.

Characterization

PXRD patterns were recorded with a Phillips PANalytical diffractometer with $\text{Cu}_{\text{K}\alpha}$ radiation ($\lambda = 1.5406 \text{ \AA}$) at a scan speed of 2° min^{-1} and a step size of 0.02° in 2θ . For measurements, samples were coated directly on XRD plates. FTIR spectra were taken with a Bruker Optics ALPHA-E spectrometer with a universal Zn–Se ATR accessory in the $600\text{--}4000 \text{ cm}^{-1}$ region or with a Diamond ATR (Golden Gate). Raman spectroscopy was carried out at room temperature with an HR 800 Raman spectrophotometer (JobinYvon HORIBA, France) by using monochromatic radiation emitted by an He–Ne laser (632 nm) operating at 20 mW. The experiment was repeated several times to verify the consistency of the spectra. TEM was carried out with Tecnai F30 FEG instrument operated at an accelerating voltage of 300 kV. Morphology and chemical composition of h-BCN were examined with Quanta 200 3D FEI scanning electron microscope. XPS measurements were carried out with a VG Micro Tech ESCA 3000 instrument at a pressure of $>1 \times 10^{-9}$ Torr (pass energy of 50 eV, an electron take-off angle of 60° , and an overall resolution of 1 eV) by using $\text{Mg}_{\text{K}\alpha}$ radiation ($h\nu = 1253.6 \text{ eV}$). The X-ray flux (power 70 W) was kept deliberately low to reduce beam-induced damage. The spectra were fitted by using a combined polynomial and Shirley-type background function. An Autosorb-iQ automatic volumetric instrument was used for low-pressure volumetric N_2 gas adsorption measurements. These meas-

measurements were performed at 77 K, maintained by a liquid nitrogen bath, with pressures ranging from 0 to 760 Torr. Ultrahigh-purity N₂ was obtained by using calcium aluminosilicate adsorbents to remove trace amounts of water and other impurities before introduction into the system.

Electrochemical measurements

EIS, CV and galvanostatic charge/discharge measurements were performed. For fabrication of the electrode, 80% of as-prepared BCN nanosheets, 10% active carbon and 10% poly(vinylidene fluoride) as binder were mixed together. Electrodes were soaked in electrolyte solution before measurements. The specific capacitance C [F g⁻¹] for a two-electrode system was calculated from galvanostatic charge/discharge data by using Equation (1)

$$C = 2I / (m \Delta V / \Delta t)$$

where I is the applied current [A], $\Delta V / \Delta t$ the slope of the discharge curve and m the average mass of active material per electrode. The factor of 2 comes from the addition of two equivalent single-electrode capacitors in a series.^[37,38]

Impedance measurements were carried out in the frequency range from 1 MHz to 0.1 Hz with an ac amplitude of 10 mV at open-circuit potential.

Acknowledgements

I.K. and J.D. acknowledge research fellowship from UGC. R.R.D. acknowledges CSIR for research fellowship. M.S. acknowledges Indo-US Science and Technology Forum, India for research fellowship. This work was supported by the Council of Scientific and Industrial Research (CSIR), India through TAPSUN program.

Keywords: boron · doping · electrochemistry · nanoparticles · nitrides

- [1] L. Ci, L. Song, C. Jin, D. Jariwala, D. Wu, Y. Li, A. Srivastava, Z. F. Wang, K. Storr, L. Balicas, F. Liu, P. M. Ajayan, *Nat. Mater.* **2010**, *9*, 430.
- [2] M. R. Lukatskaya, O. Mashtalir, C. E. Ren, Y. Dall'Agnese, P. Rozier, P. L. Taberna, M. Naguib, P. Simon, M. W. Barsoum, Y. Gogotsi, *Science* **2013**, *341*, 1502.
- [3] J. N. Coleman, M. Lotya, A. O'Neill, S. D. Bergin, P. J. King, U. Khan, K. Young, A. Gaucher, S. De, R. J. Smith, I. V. Shvets, S. K. Arora, G. Stanton, H. Y. Kim, K. Lee, G. T. Kim, G. S. Duesberg, T. Hallam, J. J. Boland, J. J. Wang, J. F. Donegan, J. C. Grunlan, G. Moriarty, A. Shmeliov, R. J. Nicholls, J. M. Perkins, E. M. Grieveson, k. Theuvsissen, D. W. McComb, P. D. Nellist, V. Nicolosi, *Science* **2011**, *331*, 568.
- [4] F. Bonaccorso, Z. Sun, T. Hasan, A. C. Ferrari, *Nat. Photonics* **2010**, *4*, 611.
- [5] R. A. Nistor, D. M. Newns, G. J. Martyna, *ACS Nano* **2011**, *5*, 3096.
- [6] M. L. Song, Z. Liu, A. L. Reddy, N. T. Narayanan, J. Taha-Tijerina, J. Peng, G. Gao, J. Lou, R. Vajtai, P. M. Ajayan, *Adv. Mater.* **2012**, *24*, 4878.

- [7] J. Han, L. L. Zhang, S. Lee, J. Oh, K. S. Lee, J. R. Potts, J. Ji, X. Zhao, R. S. Ruoff, S. Park, *ACS Nano* **2013**, *7*, 19.
- [8] C. L. Muhich, J. Y. Westcott, T. C. Morris, A. W. Weimer, C. B. Musgrave, *J. Phys. Chem. A* **2013**, *117*, 10523.
- [9] H. Liu, Y. Li, D. Zhu, *J. Mater. Chem.* **2011**, *21*, 3335.
- [10] C. H. Choi, M. W. Chung, H. C. Kwon, S. H. Park, S. I. Woo, *J. Mater. Chem. A* **2013**, *1*, 3694.
- [11] G. Fiori, A. Betti, S. Bruzzone, G. Iannaccone, *ACS Nano* **2012**, *6*, 2642.
- [12] L. W. Yin, Y. Bando, D. Golberg, A. Gloter, M. S. Li, X. Yuan, T. Sekiguchi, *J. Am. Chem. Soc.* **2005**, *127*, 16354.
- [13] L. Qin, J. Yu, S. Kuang, C. Xiao, X. Bai, *Nanoscale* **2012**, *4*, 120.
- [14] R. Riedel, J. Bill, G. Passing, *Adv. Mater.* **1991**, *3*, 551.
- [15] T. P. Fellinger, D. S. Su, M. Engenhorst, D. Gautam, R. Schlogl, M. Antonietti, *J. Mater. Chem.* **2012**, *22*, 23996.
- [16] M. Kawaguchi, *Adv. Mater.* **1997**, *9*, 615.
- [17] S. Wang, L. Zhang, L. Xia, A. Roy, D. W. Chang, J. B. Baek, L. Dai, *Angew. Chem. Int. Ed.* **2012**, *51*, 4209; *Angew. Chem.* **2012**, *124*, 4285.
- [18] M. Terrones, D. Golberg, N. Grobert, T. Seeger, M. Reyes-Reyes, M. Mayne, R. Kamalakaran, P. Dorozhkin, Z. C. Dong, H. Terrones, M. Ruhle, Y. Bando, *Adv. Mater.* **2003**, *15*, 1899.
- [19] K. Raidongia, A. Nag, K. P. S. S. Hembram, U. V. Waghmare, R. Datta, C. N. R. Rao, *Chem. Eur. J.* **2010**, *16*, 149.
- [20] Y. Zhang, H. Gu, K. Suenaga, S. Iijima, *Chem. Phys. Lett.* **1997**, *279*, 264.
- [21] J. Yu, J. Ahn, S. F. Yoon, Q. Zhang, B. Gan, K. Chew, M. B. Yu, X. D. Bai, E. G. Wang, *Appl. Phys. Lett.* **2000**, *77*, 1949.
- [22] C. Y. Zhi, J. D. Guo, X. D. Bai, E. G. Wang, *J. Appl. Phys.* **2002**, *91*, 5325.
- [23] S. Enouz-Védrenne, O. Stephan, M. Glerup, J. L. Cochon, C. Colliex, A. Loiseau, *J. Phys. Chem. C* **2008**, *112*, 16422.
- [24] F. Piazza, J. E. Nocua, A. Hidalgo, J. De Jesus, R. Velazquez, B. L. Weiss, G. Morell, *Diamond Relat. Mater.* **2005**, *14*, 965.
- [25] W. Lei, D. Portehault, R. Dimova, M. Antonietti, *J. Am. Chem. Soc.* **2011**, *133*, 7121.
- [26] T. Zhang, G. Wen, X. Huang, B. Zhong, H. Yu, *CrystEngComm* **2010**, *12*, 3506.
- [27] X. Liu, X. Jia, Z. Zhang, M. Zhao, W. Guo, G. Huang, H. Ma, *Cryst. Growth Des.* **2011**, *11*, 1006.
- [28] W. Lei, S. Qin, D. Liu, D. Portehault, Z. Liu, Y. Chen, *Chem. Commun.* **2013**, *49*, 352.
- [29] E. Iyyamperumal, S. Wang, L. Dai, *ACS Nano* **2012**, *6*, 5259.
- [30] S. Umrao, T. K. Gupta, S. Kumar, V. K. Singh, M. K. Sultania, J. Hwan Jung, I. K. Oh, A. Srivastava, *ACS Appl. Mater. Interfaces* **2015**, *7*, 19831.
- [31] Q. H. Yang, P. X. Hou, M. Unno, S. Yamauchi, R. Saito, T. Kyotani, *Nano Lett.* **2005**, *5*, 2465.
- [32] T. Ogi, Y. Kaihatsu, F. Iskandar, W. N. Wang, K. Okuyama, *Adv. Mater.* **2008**, *20*, 3235.
- [33] H. Konno, T. Ito, M. Ushiro, K. Fushimi, K. Azumi, *J. Power Sources* **2010**, *195*, 1739.
- [34] H. Guo, Q. Gao, *J. Power Sources* **2009**, *186*, 551.
- [35] A. Nag, K. Raidongia, K. P. S. S. Hembram, R. Datta, U. V. Waghmare, C. N. R. Rao, *ACS Nano* **2010**, *4*, 1539.
- [36] S. Mondal, A. K. Banthia, *Adv. Mater. Res.* **2007**, *29*, 199.
- [37] M. Wahid, D. Puthusseri, D. Phase, S. Ogale, *Energy Fuels* **2014**, *28*, 4233.
- [38] Q. Wang, N. Plylahan, M. V. Shelke, R. R. Devarapalli, M. Li, P. Subramanian, T. Djenizian, R. Boukherroub, S. Szunerits, *Carbon* **2014**, *68*, 175.

Received: December 31, 2015

Published online on April 13, 2016